Acta Oceanol. Sin., 2018, Vol. 37, No. 11, P. 88–95
DOI: 10.1007/s13131-018-1258-5
http://www.hyxb.org.cn
E-mail: hyxbe@263.net

An experimental study on oil droplet size distribution in subsurface oil releases

LI Jianwei[1, 2], AN Wei[2*], GAO Huiwang[1], ZHAO Yupeng[2], SUN Yonggen[3*]

[1] Key Laboratory of Marine Environment and Ecology, Ministry of Education of China, Ocean University of China, Qingdao 266100, China

[2] China Offshore Environmental Services Ltd., Tianjin 300452, China

[3] The First Institute of Oceanography, State Oceanic Administration, Qingdao 266061, China

Received 7 May 2018; accepted 9 July 2018

Abstract

Oil droplet size distribution (ODSD) plays a critical role in the rising velocity and transport of oil droplets in subsurface oil releases. In this paper, subsurface oil release experiments were conducted to study ODSD under different experimental conditions in a laboratory water tank observed by two high-speed cameras in March and April 2017. The correlation formulas Oh=10.2Re^{-1} and Oh=39.2Re^{-1} (Re represents Reynolds number and Oh represents Ohnesorge number) were established to distinguish the boundaries of the three instability regimes in dimensionless space based on the experimental results. The oil droplet sizes from the experimental data showed an excellent match to the Rosin–Rammler distribution function with determination coefficients ranging from 0.86 to 1.00 for Lvda 10-1 oil. This paper also explored the influence factors on and change rules of oil droplet size. The volume median diameter d_{50} decreased steadily with increasing jet velocity, and a sharp decrease occurred in the laminar-breakup regime. At Weber numbers (We) <100, the orifice diameter and oil viscosity appeared to have a large influence on the mean droplet diameter. At 100<We<1 000, the oil viscosity appeared to have a larger influence on the relative mean droplet diameter.

Key words: oil droplet size distribution, subsurface oil releases, Rosin–Rammler distribution

Citation: Li Jianwei, An Wei, Gao Huiwang, Zhao Yupeng, Sun Yonggen. 2018. An experimental study on oil droplet size distribution in subsurface oil releases. Acta Oceanologica Sinica, 37(11): 88–95, doi: 10.1007/s13131-018-1258-5

1 Introduction

Releases of subsurface oil into the water column often occur with the development of offshore oil and gas exploration, which may be caused by vessel collisions, well blowout or pipeline rupture (Zhu et al., 2017). Subsurface oil releases may pose a major threat to the marine environment, such as in the Deepwater Horizon (DWH) blowout, which released approximately 4.93 million barrels of crude oil (Li et al., 2016). During the DWH blowout, the larger oil droplets took a few hours to rise to the surface, while some smaller droplets could stay in the water column for weeks or months (Brandvik et al., 2013; Ryerson et al., 2012; Geng et al., 2016). Previous studies showed that oil droplet size distribution (ODSD) played an important role in the rising velocity and transport of the released oil in subsurface oil releases (Johansen et al., 2013; Chen et al., 2016; Brakstad et al., 2015; Zheng and Yapa, 2000), and the ODSD determined when and where oil rose to the surface, and even whether the oil rose to the surface or not (Niu et al., 2011). Furthermore, ODSD could also affect the horizontal movement and toxic effects of oil droplets in the water column (Nissanka and Yapa, 2016). In order to study the ODSD, *in situ* and laboratory some subsurface oil release experiments were conducted. In June 2000, the Deep Spill experiment was conducted to observe ODSD at a depth of 844 meters in the Norwegian Sea (Johansen et al., 2001). In addition, ODSD was analyzed by laboratory experiments in a water tank with a length of 0.5 m, a width of 0.5 m and a height of 1.3 m, and certain influence factors were considered (Masutani and Adams, 2004). Experiments with subsurface oil releases with and without dispersant were conducted in the Tower Basin, which had tested different oil types at several temperatures and with different dispersants (Brandvik et al., 2013). The application of a subsurface dispersant decreased the average droplet diameter and conversely increased the number of droplets observed in the water column (Aprin et al., 2015). Subsurface oil release experiments considering the various forces affecting the migration of the droplets were studied in an Ohmsett tank with a length of 203 m, a width of 20 m, and a height of 3.4 m (Zhao et al., 2016).

In addition to these experiments, some prediction models for ODSD were built to understand the droplet size distribution. A two-step Rosin-Rammler scheme was introduced by developing a Reynolds-number scaling approach to predict droplet size distribution (Li et al., 2016). Droplet size distribution was studied by a Weber number scaling approach and a maximum entropy formalism approach (Chen and Yapa, 2003, 2007). Subsequently, a modified Weber number scaling approach was developed with chemical dispersants being applied (Johansen et al., 2013). A population model was established coupled with the plume model, and breakup and coalescence were the most important processes during the first meters of the oil jet, where turbulence was dominant (Bandara and Yapa, 2011). Both interfacial tension and oil viscosity were considered in the VDROP model to resist the breakup of droplets due to turbulence (Zhao et al., 2014). The

Foundation item: The National Key Research and Development Program of China under contract No. 2016YFC1402303.
*Corresponding author, E-mail: anwei2@cnooc.com.cn; sunyonggen@126.com

model oil droplets was introduced by using an improved theoretical method and agreed well with the experimental data (Nissanka and Yapa, 2016).

Although the previous studies of ODSD have been conducted by experiments and model simulations, but the factors to control ODSD are not clear. In this paper, experiments in water tank and the image analysis are applied to estimate the size of the dispersed droplet phase. We focused on the ODSD of subsurface oil releases through the use of five orifice diameters, two oil types, two ambient fluids, and different injection velocities to understand the role of jet velocity, orifice diameter, oil types and ambient fluids on ODSD.

2 Materials and methods

2.1 *Experimental setup*

To study oil release behaviors and the distribution of oil droplet size, some water tanks were built in which many experiments were conducted (Tang and Masutani, 2003; Johansen et al., 2013; Zhao et al., 2016). In this study, experiments on subsurface oil releases were conducted in a 2.0 m tall by 1.0 m×1.0 m square water tank located at The First Institute of Oceanography (SOA, China). The tank had an effective operating depth of 1.8 m. Figure 1a presents the schematic diagram of experimental setup consisting of the oil injection system, tank body and control system. The oil injection system structures were relatively complex and were made essentially of an oil reservoir, gear pump, oil pipeline, nozzles, temperature sensor, pressure sensor, flowmeter and so on. The five injection nozzles had diameters of 1.30, 1.95, 3.33, 4.41, 5.07 mm and were placed at the bottom of the tank. In the experiment, crude oil in a small (approximately 2.5 liters) reservoir was heated to a set temperature with constant stirring. A pulseless gear pump (BB-B10Y) coupled to a variable-speed motor drew oil into the pipeline and was used to adjust jet velocity. The oil was discharged vertically upward as a constant-flow oil jet through different nozzles into the water tank. The temperature, pressure and flow data were detected in real time by sensors. The flowmeter had an effective monitoring range of 0.3–500 L/h with an error of 0.2%. Two high-speed industrial cameras were employed to measure oil droplet size. All setup parameters were controlled by an industrial computer to improve accuracy.

2.2 *Experimental materials*

The subsurface oil release experiments were conducted in the water tank in March and April 2017. Two crude oil types (Lvda10–1 and Fenjin) were investigated under different conditions, resulted in 62 runs for the entire experimental design. Table 1 presents the physical and chemical properties of the two crude oils. The specific gravity and viscosity of crude oil varies at different temperatures, so we deduced the density-temperature curve and kinematic viscosity-temperature curve. The interfacial tensions were 25.9 mN/m and 26.6 mN/m between seawater and the Lvda10–1 oil and Fenjin oil, respectively. In contrast, the interfacial tension was 17.5 mN/m between freshwater and the Lvda10–1 oil. To more closely imitate the real environment, the seawater for our experiment was from the coast sea of Qingdao, which had a conductivity and density of 47.1 mS/cm and 1 023 kg/m^3, respectively. All experiments were carried out at mean water temperature T_{water}=16°C and the oil temperature was set to T_{oil}= (40±0.1)°C to simulate oil releases from submarine pipelines. The injection velocity ranged from 0.04 m/s to 11.5 m/s. The settings for experiments in the water tank are listed in Table 2.

Table 1. Physical and chemical properties of the two crude oils

Items	Lvda10–1	Fenjin
Density-temperature curve/(20–40°C)	ρ=950.71exp (–8×10^{-4}T)	ρ=847.9exp (–10^{-3}T)
Kinematic viscosity-temperature curve/(20–40°C)	μ=2 770.8exp (–0.079T)	μ=19.173exp (–0.035T)
IFT of the oil-seawater/mN·m^{-1}	25.9	26.6
IFT of the oil-freshwater/mN·m^{-1}	17.5	–

Note: ρ—density, kg/m^3, μ—kinematic viscosity, mm^2/s, T—temperature, °C

Table 2. Experimental release conditions in the tank

Parameters	Values
Oil sample	Lvda10-1, Fenjin
Nozzles diameter/mm	1.30, 1.95, 3.33, 4.41, 5.07
Jet velocity/m·s^{-1}	0.04–11.50
Water	seawater, fresh water
Water temperature/°C	16
Oil temperature/°C	40±0.1

2.3 *Data collection and analysis*

In previous studies, the dispersed oil droplet size was analyzed by using a LISST-100X (Sequoia Scientific Inc. Seattle, WA), but its measurements were in the range of 2.5–500 μm (Li et al., 2011; Tang and Masutani, 2003; Johansen et al., 2013; Zhao et al., 2014). In addition, the LISST-100X could obtain real-time data, but it led to repetitive calculation for smaller oil droplets, which had lower rising velocity, and it could produce an error in the oil droplet size.

Image analysis used for droplet size measurements was typically the method of choice that can provide qualitative insight and quantitative data (Tang and Masutani, 2003; Neto et al., 2008). Currently, the resolution of high-speed imaging systems can reach 10 μm (Brandvik et al., 2013; Aprin et al., 2015). Several tests were conducted, and image analysis was able to measure single droplets in a dispersed distribution. One of the advantages of image analysis was that we could select the appropriate images manually to avoid duplicate calculations.

In the experiments, dispersed oildroplet size was measured by two industrial cameras, which were calibrated using a C4 eyepiece micrometer scale. The cameras were used to monitor the process of oil droplet formation and flow pattern in real time, and they were placed at a height of 150 cm above the nozzle. To improve visual identification of oil droplets and the resolution of the images, the high-speed, high-resolution camera (ICX625) were placed inside the water. They were able to capture droplet motion at 17 frames per second (fps), for which the frame resolution was set to a maximum of 2 456×2 058 pixels and the lens resolution was 5.8 μm. By putting it in the water, the image analysis succeeded in discerning the dense droplets because it could separate individual droplets from each other. We used the backlight to provide lighting system which was LED lights (Fig. 1b). It has 15 W power and 6 500 K color temperature. The distance between the lighting source and the camera is about 100 mm, and lighting system could penetrate the oil plume. Under these conditions, images of oil droplets and their size distribution were clearly captured by the camera (Fig. 1c). The other camera (CMV2000), used for the larger oil droplets, was placed outside the tank. It was able to capture 50 fps for which the frame resolution was set to a maximum of 2 048×1 088 pixels, and the lens resolution was 200 μm. The observation of oil-droplet size distribution lasted at least 2 min to obtain a sufficient number of images. Video images were subsequently analyzed frame-by-frame by

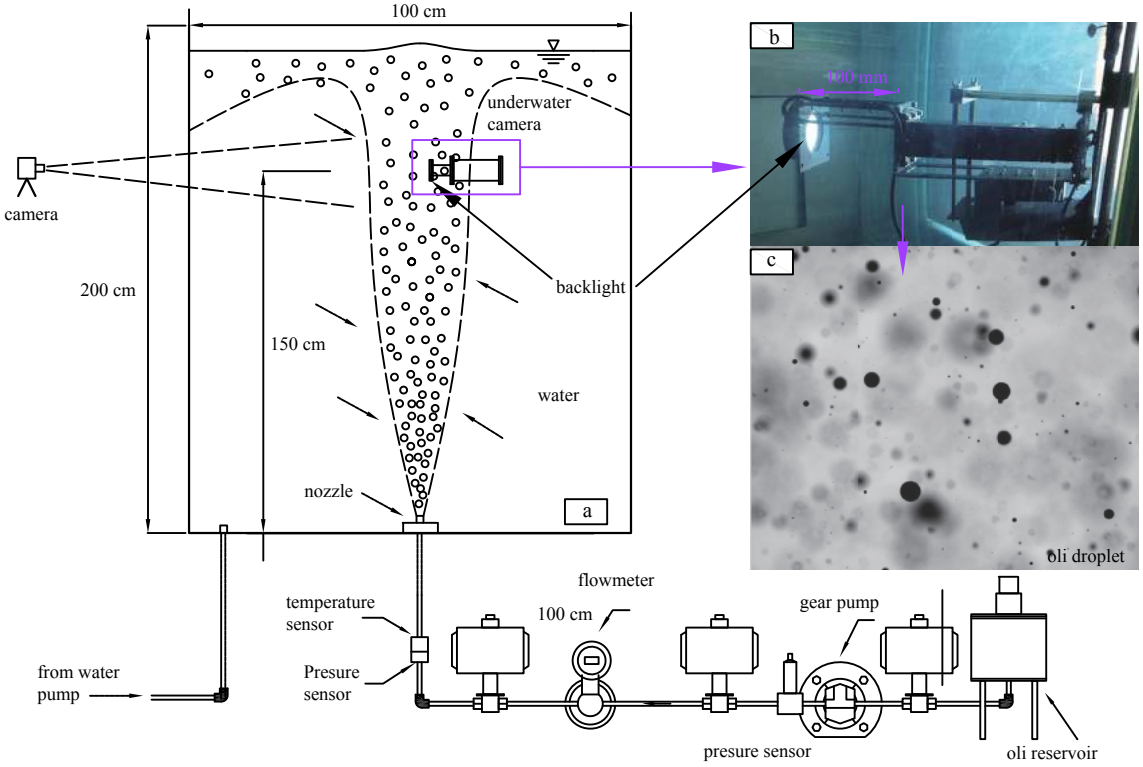

Fig. 1. Schematic diagram of the experimental water tank.

soft Image-Pro Plus 6.0 to computer oil droplet size. Then, we calculated the critical size of the oil droplets d_e and the spread exponent m by a Rosin-Rammler distribution function.

3 Results and discussion

3.1 *Regimes of droplet formation*

For the purpose of observing the transition process of regimes of droplet formation, experiments were performed by increasing the jet velocity while keeping other parameters fixed to increase the relative Reynolds number between phases in a stepwise manner. Figure 2 shows experimental images of oil discharged into water at different jet velocity conditions from the 1.95 mm nozzle for Lvda10–1 by using the high-resolution camera. It could be found that the mechanism of oil droplet formation and droplet size were dynamically evolving in time. Meanwhile, as previously observed from the breakup experiments (Johansen et al., 2013), the droplet formation regime was divided into three types, i.e., the laminar breakup, transitional breakup and atomization-breakup regimes. In the laminar-breakup regime (the first four images of Fig. 2), a stable laminar jet formed at the nozzle, and the jet rose to a certain height and then broke up into single droplets. In the atomization-breakup regime (the last two images of Fig. 2), the jet was fully turbulent and eventually disrupted intensely into a large number of smaller droplets, rising upwards as a dispersion. The transitional-breakup regime (the remaining two images of Fig. 2) was located in the transition domain. Moreover, it was clear from Fig. 2 that oil-droplet formation occurred by three absolutely different development regimes.

Oil droplet breakup regimes were represented by two dimensionless numbers (Li et al., 2016; Masutani and Adams, 2004; Peng et al., 2009; Johansen et al., 2013), the Reynolds number (Re) and the Ohnesorge number (Oh). The relative Reynolds number, based on the relative velocity, was introduced to account for the integration effects of the relative motion of the two phases and was expressed in Eq. (1). Oh represented the ratio of viscous forces to surface tension as expressed in Eq. (2).

$$Re = \frac{\rho U d}{\mu}, \tag{1}$$

$$Oh = \frac{\mu}{(\rho\sigma d)^{1/2}}, \tag{2}$$

where ρ is the density of the jet fluid, U is the jet velocity, d is the orifice diameter, μ is the dynamic viscosity of the jet fluid, and σ is the interfacial tension between oil and water.

Figure 3 exhibits a plot of Oh versus Re for our data set, where the data points were illustrated by their corresponding breakup regimes. The boundaries of the breakup regimes could be related to a linear relationship of the form Oh=cRe^{-1} (Tang and Masutani, 2003; Masutani and Adams, 2004) where c was a constant of proportionality. The dashed line drawn in the diagram showed the boundary. The correlation equation Oh=10.2Re^{-1} was the boundary between the laminar and transitional breakup. In addition, the correlation equation Oh=39.2Re^{-1} was the boundary between the transitional and atomization breakup. The constant c was different from previous studies (Tang and Masutani, 2003). One cause for this difference was that droplet breakup may be caused by different mechanisms depending on the properties of the fluid.

3.2 *Droplet size distribution*

Two common methods to present the droplet size distributions are by the log-normal distribution function or by the Rosin-Rammler distribution function (Johansen et al., 2003, 2013; Lefe-

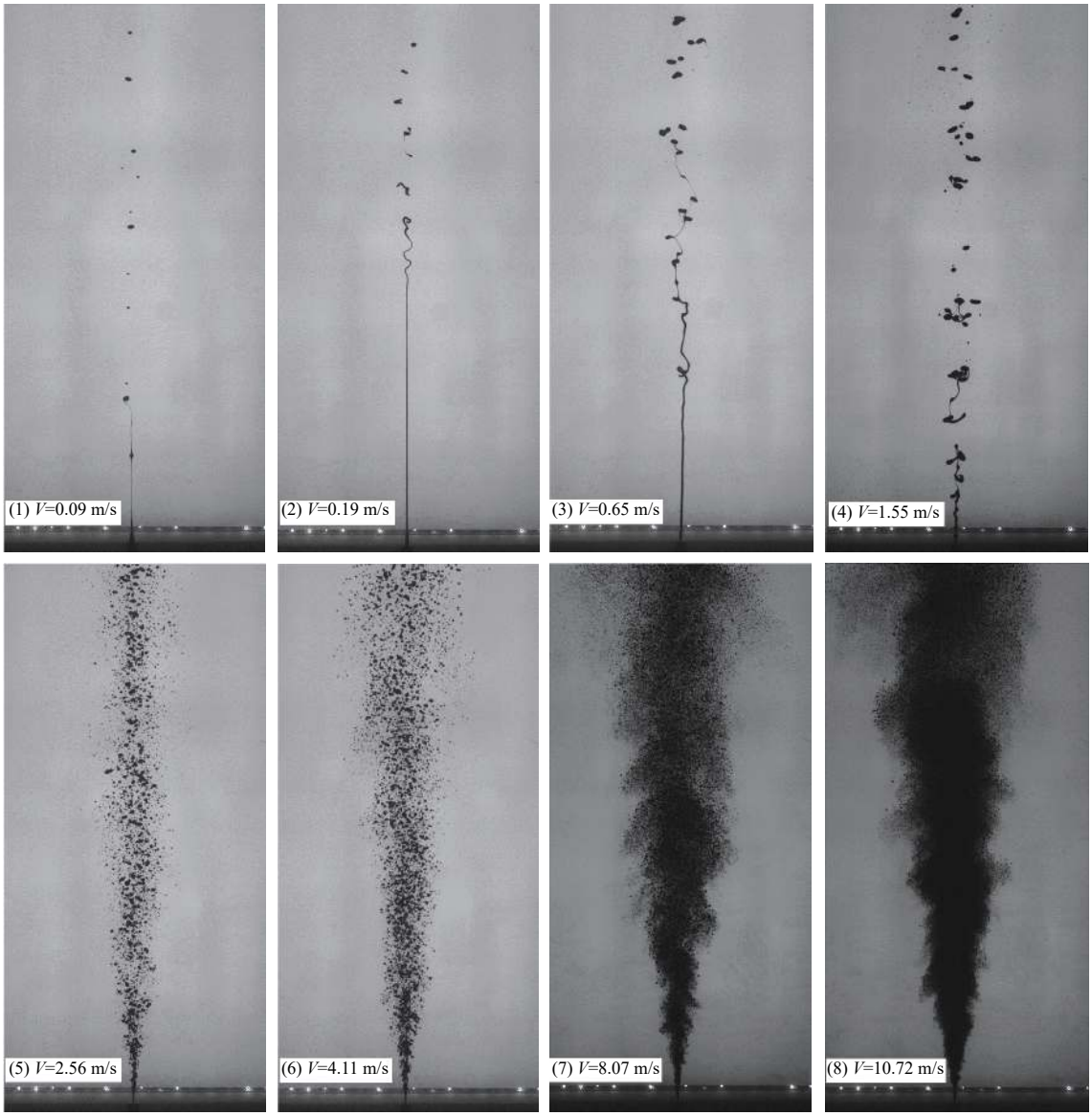

Fig. 2. Images of oil discharged into water from a 1.95 mm nozzle.

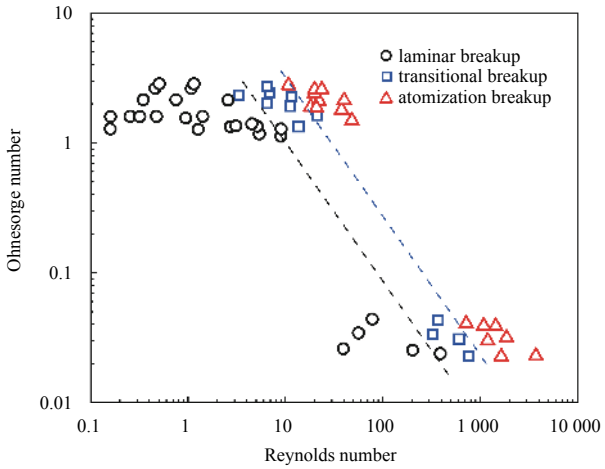

Fig. 3. *Oh* versus *Re* scatter plot of experimental runs and their corresponding breakup regimes.

bvre, 1989). The former can be understood as a normal distribution of the logarithms of the droplet sizes. The latter is a two-parameter distribution function, defined in terms of a critical particle diameter d_e corresponding to a certain cumulative volume fraction $R(d)$, and a spreading parameter m. The cumulative volume distribution was given as shown in the following Eq. (3). From Eq. (3), it is clear that the sole size distribution of the droplets is produced when m and d_e are specified. Equation (3) can be varied as a logarithmic form as shown in the following Eq. (4).

$$R(d) = 1 - \exp\left[-\left(\frac{d}{d_e}\right)^m\right], \tag{3}$$

where $R(d)$ is the cumulative volume fraction (%), d is the particle size (μm), d_e is the critical particle diameter (μm) when d=d_e, and m is the spread exponent of particle sizes.

$$\ln\{-\ln[1 - R(d)]\} = m\ln d - m\ln d_e. \tag{4}$$

It can be seen from Eq. (4) that the regression is a line in the

ln(d) and ln{–ln[1–$R(d)$]} coordinates provided that the droplet size satisfies the Rosin-Rammler distribution function. The exponent m and the critical diameter d_e can be specified as the slope and the intercept of this inclined line, respectively.

Table 3 shows the corresponding the exponent m, critical particle diameter d_e and the determination coefficients R^2 of Rosin-Rammler distribution function for Lvda10–1 oil under different experimental conditions. For the Rosin-Rammler distribution, the critical diameter ranged from 10.7 to 3 899.7 μm, with a spreading coefficient m ranging from 0.37 to 1.18. The R^2 of the regression lines of the Rosin-Rammler distribution was from 0.86 to 1.00, suggesting that the oil droplet size from the experimental data showed an excellent match to the Rosin–Rammler distribution. Figure 4 illustrated the regression line and the size distribution of oil droplets calculated by the Rosin-Rammler distribution function under double logarithmic coordinates. To display this well display, a portion of the data is listed in Fig. 4. It could be found that comparison of the oil droplet size with the Rosin-Rammler distribution function showed good agreement.

Table 3. The corresponding values of the spread exponent m, critical particle diameter d_e and the determination coefficients of the Rosin-Rammler distribution function

Orifice diameter/mm	Jet velocity/ m·s^{-1}	m	Critical diameter/μm	R^2
1.30	0.21	1.01	2 793.1	0.94
	0.48	0.96	3 248.3	0.91
	1.14	0.54	1 316.0	0.88
	2.59	0.63	1 237.3	0.92
	4.37	0.90	969.6	0.98
	6.95	0.47	27.5	0.99
	7.50	0.40	10.7	0.98
	8.85	0.64	68.4	1.00
	10.44	0.63	50.9	0.99
1.95	0.09	0.73	1 519.2	0.93
	0.19	0.71	1 617.7	0.86
	0.65	0.63	1 419.1	0.99
	1.55	0.67	1 825.6	0.90
	2.56	0.87	959.7	0.97
	4.11	0.78	630.4	0.98
	4.63	0.49	51.4	0.98
	8.07	0.41	11.1	1.00
	10.72	0.73	42.6	1.00
3.33	0.04	1.17	3 899.7	0.95
	0.07	0.80	2 425.9	0.87
	0.21	0.68	2 287.0	0.88
	0.58	0.62	2 258.3	0.88
	0.94	0.78	2 204.5	0.96
	1.66	0.96	1 114.0	0.97
	3.16	0.37	11.0	0.95
	6.52	0.53	25.3	0.99
	11.09	0.55	15.5	1.00
4.41	0.02	1.18	3 271.3	0.95
	0.04	1.08	3 379.5	0.89
	0.12	0.89	3 108.5	0.87
	0.33	0.75	2 779.8	0.90
	0.55	0.64	1 888.4	0.95
	0.92	0.87	1 913.3	0.99
5.07	0.02	1.17	2 734.3	0.92
	0.12	0.47	381.2	0.90
	0.27	0.71	1 787.5	0.94
	0.47	0.86	1 801.5	0.96
	0.74	0.99	1 847.8	0.98

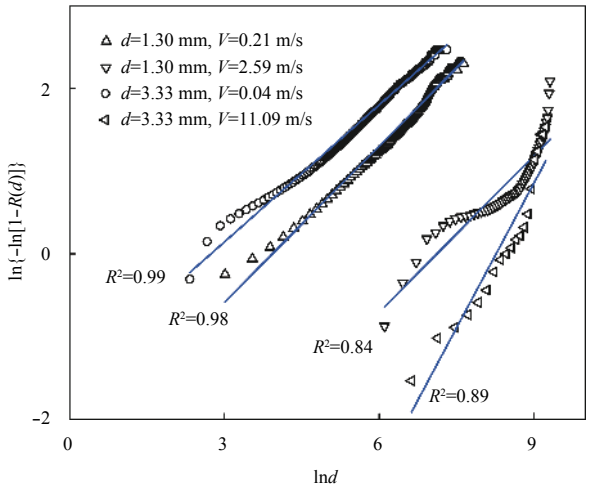

Fig. 4. Expressions of linear regression for Lvda10-1 oil.

Figure 5 demonstrates the variation-of-spread exponent m and the critical diameter of ODSD with increasing jet velocity for the 1.30 mm nozzle diameter for Lvda10–1 oil. It could be found from Fig. 5 that the spread exponent and critical diameter varied with the jet velocity. In the laminar-breakup regime of droplet formation, the spread exponent decreased with increasing jet velocity, which varied from 1.01 to 0.54. In the transitional-breakup regime, the spread exponent increased with increasing jet velocity, which varied from 0.54 to 0.90. As the jet velocity increased, after entering the atomization-breakup regime the spread exponent first decreased and then increased, and ranged from 0.90 to 0.40. It could also be seen that the critical diameter decreased continuously according to increasing jet velocity, which varied from 3 248.3 μm to 10.7 μm. In addition to this, the values of the spread exponent m and critical diameter from Table 3 definitely showed a consistent change trend. This implied that the uniformity and characteristic diameter of ODSD may have been related to the jet velocity. The most likely cause for the variation was the transformation between the balance and imbalance of gravity, buoyancy, interfacial tension and viscous force. Meanwhile, small droplets were mainly caused by high turbulence at the release point at a higher jet velocity (Yapa et al., 2012).

3.3 *Influence factors of droplet size*

Jet velocity, nozzle diameter, ambient fluid and oil properties

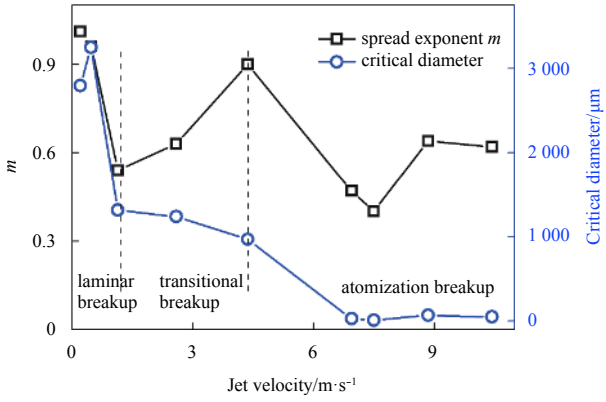

Fig. 5. Variation of the spread exponent and the critical diameter.

all had effects on the size distribution of the droplets (Masutani and Adams, 2004). Because there was a wide distribution of droplet size, the volume median diameter of the droplets d_{50} could reflect the droplet size distribution (Zhao et al., 2014; Li et al., 2016). In this study, d_{50} was also used to research the influence factors of droplet size distribution. The computing method was the following equation:

$$d_{50} = d_e \sqrt[m]{-\ln 0.5}, \quad (5)$$

where d_{50} is the volume median diameter, d_e is critical particle diameter, and m is the spread exponent.

3.3.1 *Jet velocity*

Figure 6 shows a plot of the results of the volume median diameter d_{50} vs. jet velocity for Lvda10–1 oil. It could be found that d_{50} decreased steadily with increasing jet velocity. This can also be explained by the fact that the jet velocity affected the turbulence, which influences the ODSD (Yapa et al., 2012) and that the jet velocity could yield oil droplet size distributions containing smaller droplets. A sharp decrease occurred from 2 848 to 670 μm in the laminar-breakup regime, followed by a milder decrease in the transitional-breakup regime ranging from 759.1 to 24.4 μm, with essentially no change in the atomization-breakup regime. There was a reason that the ODSD was shifted towards smaller sizes with larger jet velocity. In other words, the larger the droplet was, the more likely it was to break up.

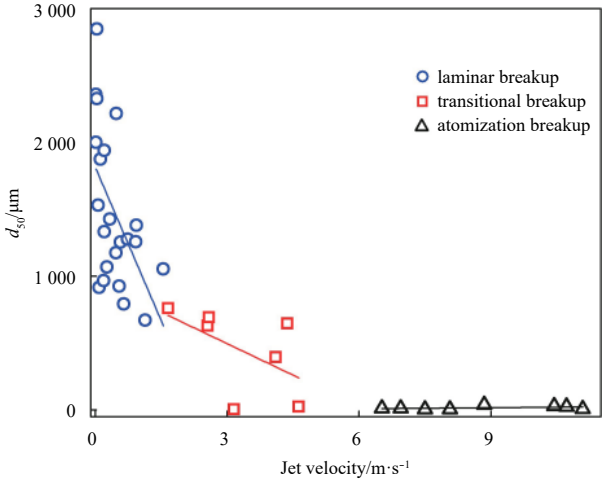

Fig. 6. The volume median diameter under different jet velocity for Lvda10-1.

3.3.2 *Orifice diameter*

Figure 7 demonstrates a plot of the relative median droplet diameter (d_{50}/D) vs. the Weber number (We), where D is the size of the nozzle diameter. These data were from the injection of Lvda10–1 into seawater through difference orifices. It was clear that a smaller orifice produced a modestly larger value of d_{50}/D at low We, but this effect diminished with increasing values of We. At 100<We<1 000, the orifice diameter appeared to have a smaller influence on the mean droplet diameter. However, at We>1 000, the value of d_{50}/D had almost no effect for different orifice diameters. This suggested that the formation mechanism of the small droplets became relatively independent once a threshold droplet diameter was reached. The reason was that surface instabilities may be sensitive to the orifice diameter at lower values of We.

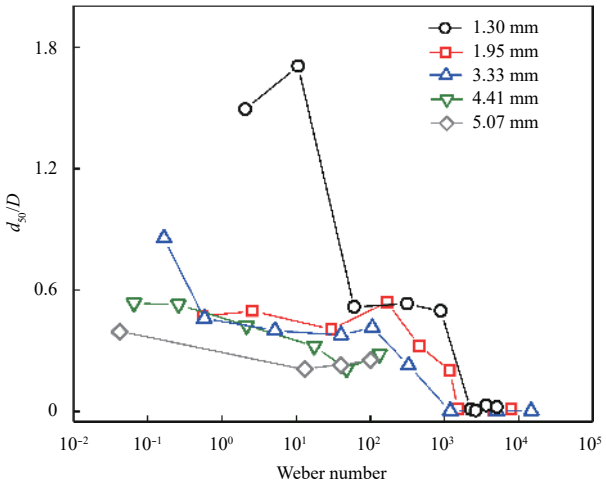

Fig. 7. The relative median droplet diameter vs. the We for different Orifices

3.3.3 *Types of oil and fluid*

Figure 8 shows a plot of d_{50}/D vs. We for different oil types from a 3.33 mm orifice. These data corresponded to two oil types with kinematic viscosities that ranged over two orders of magnitude. The viscosity of the Fenjin oil was 8.2 mm^2/s, but the viscosity of the Lvda10–1 oil was 464.7 mm^2/s. At low values of We, the jet viscosity seemed to have little effect on the relative median droplet diameter. As We increased, the relative median droplet diameter appeared to increase slightly with the oil viscosity. At 1<We<1 000, the oil viscosity appeared to have a larger influence on the relative mean droplet diameter. At We>1 000, the oil viscosity appeared to have a smaller influence on the relative mean droplet diameter.

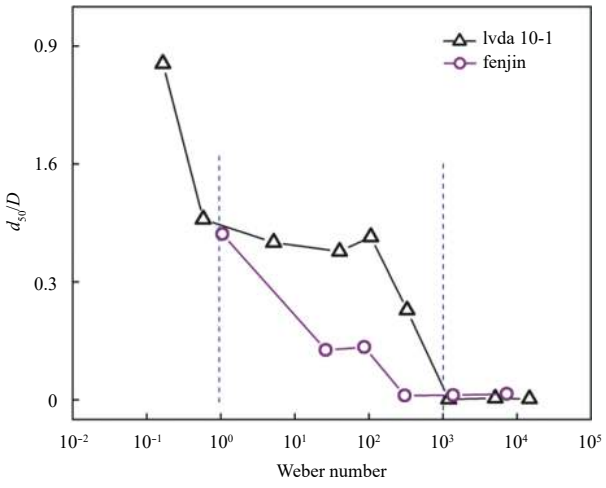

Fig. 8. The relative median droplet diameter vs. the We for the two oils.

The effect of two different values of interfacial tension, i.e., 25.9 and 17.5 mN/m on the volume median diameter was analyzed. Figure 9 shows a plot of d_{50} vs. the jet velocity for different ambient fluids from a 1.95 mm orifice. As shown in Fig. 9, the median droplet size ranges from 4.6 to 1 053.9 μm for seawater, but the median droplet size ranges from 6.7 to 698.7 μm for fresh water. This implied a change in the mean droplet diameter with in-

creasing jet velocity for different values of interfacial tension. The mean droplet diameter was larger in seawater than in fresh water. At a low jet velocity, the interfacial tension seemed to have a larger effect on the median droplet diameter. When the jet velocity was >8 m/s, the interfacial tension had little effect on the droplet diameter.

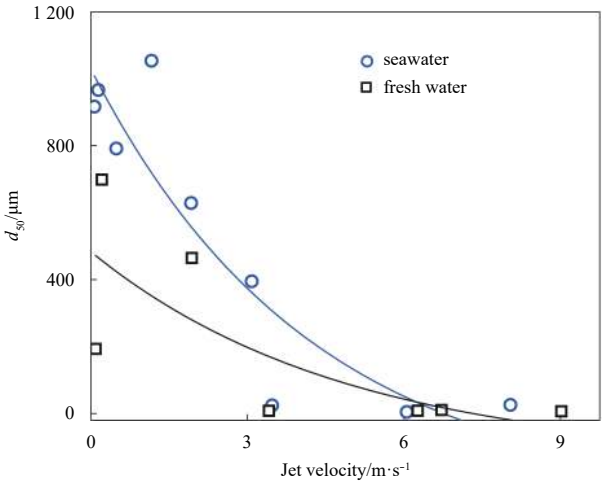

Fig. 9. The median droplet diameter vs. the jet velocity for different ambient fluids.

4 Conclusions

Subsurface oil release experiments have been performed to study ODSD under different experimental conditions in a laboratory water tank. We acquired experimental data for subsurface oil releases through orifices of five different diameters, two oil types, two ambient fluids, and different injection velocities. Detailed measurements of the size distribution and of the formation of oil droplets were obtained, and the main conclusions are as follows:

(1) Regimes of oil droplet formation were divided into three different developing regimes: laminar breakup, transitional breakup and atomization-breakup regimes. In addition, the correlation formulas of the boundaries were established based on the Reynolds number and the Ohnesorge number, which were Oh=10.2 Re^{-1} and Oh=39.2 Re^{-1}, respectively.

(2) The oil-droplet size showed an excellent agreement with the Rosin–Rammler distribution function with determination coefficients ranging from 0.86 to 1.00 for Lvda10–1 oil. The critical diameter decreased continuously according to increasing jet velocity, varying from 3 248.3 to 10.7 μm. In addition, the spread exponent changed differently in each of the three droplet formation regimes.

(3) Based on the experimental data analysis, the jet velocity, orifice diameter, ambient fluid and oil type all had an effect on ODSD. The volume median diameter d_{50} decrease steadily with increasing jet velocity, and a sharp decrease occurred in the laminar-breakup regime. At We<100, the orifice diameter and oil viscosity appeared to have a larger influence on the mean droplet diameter. Moreover, at 100<We<1 000, the oil viscosity appeared to have a larger influence on the relative mean droplet diameter.

Acknowledgements

The authors want to acknowledge the helpful guidance and advice from Yu Shun from The First Institute of Oceanography, State Oceanic Administration. They also acknowledge the constructive and valuable comments and suggestions of the reviewer and the editor.

References

Aprin L, Heymes F, Lauret P, et al. 2015. Experimental characterization of the influence of dispersant addition on rising oil droplets in water column. Chemical Engineering Transactions, 43: 2287–2292

Bandara U C, Yapa P D. 2011. Bubble sizes, breakup, and coalescence in deepwater gas/oil plumes. Journal of Hydraulic Engineering, 137(7): 729–738, doi: 10.1061/(ASCE)HY.1943-7900.0000380

Brakstad O G, Nordtug T, Throne-Holst M. 2015. Biodegradation of dispersed Macondo oil in seawater at low temperature and different oil droplet sizes. Marine Pollution Bulletin, 93(1–2): 144–152

Brandvik P J, Johansen Ø, Leirvik F, et al. 2013. Droplet breakup in subsurface oil releases-part 1: experimental study of droplet breakup and effectiveness of dispersant injection. Marine Pollution Bulletin, 73(1): 319–326, doi: 10.1016/j.marpolbul.2013.05.020

Chen Fanghui, Yapa P D. 2003. A model for simulating deep water oil and gas blowouts - Part II: Comparison of numerical simulations with "Deepspill" field experiments. Journal of Hydraulic Research, 41(4): 353–365, doi: 10.1080/00221680309499981

Chen Haibo, An Wei, You Yunxiang, et al. 2016. Modeling underwater transport of oil spilled from deepwater area in the South China Sea. Chinese Journal of Oceanology and Limnology, 34(1): 245–263, doi: 10.1007/s00343-015-4230-7

Chen Fanghui, Yapa P D. 2007. Estimating the oil droplet size distributions in deepwater oil spills. Journal of Hydraulic Engineering, 133(2): 197–207, doi: 10.1061/(ASCE)0733-9429(2007)133:2(197)

Geng Xiaolong, Boufadel M C, Ozgokmen T, et al. 2016. Oil droplets transport due to irregular waves: development of large-scale spreading coefficients. Marine Pollution Bulletin, 104(1–2): 279–289

Johansen Ø, Brandvik P J, Farooq U. 2013. Droplet breakup in subsea oil releases – part 2: predictions of droplet size distributions with and without injection of chemical dispersants. Marine Pollution Bulletin, 73(1): 327–335, doi: 10.1016/j.marpolbul.2013.04.012

Johansen Ø, Jensen H V, Daling P. 2001. Deep spill JIP experimental discharges of gas and oil at Helland Hansen—June 2000. SINTEF Report. Norway: SINTEF (请核对年份信息)

Johansen Ø, Rye H, Cooper C. 2003. DeepSpill--field study of a simulated oil and gas blowout in deep water. Spill Science & Technology Bulletin, 8(5–6): 433–443

Lefebvre A H. 1989. Atomization and Sprays. New York: Hemisphere Pub. Corp, 421

Li Zhengkai, Lee K, Kepkey P, et al. 2011. Monitoring dispersed oil droplet size distribution at the gulf of Mexico deepwater horizon spill site. International Oil Spill Conference Proceedings, 2011(1): abs377

Li Pu, Weng Linlu, Niu Haibo, et al. 2016. Reynolds number scaling to predict droplet size distribution in dispersed and undispersed subsurface oil releases. Marine Pollution Bulletin, 113(1–2): 332–342

Masutani S M, Adams E E. 2004. Liquid droplet contaminant plumes in the deep ocean. Japanese Journal of Multiphase Flow, 18(2): 135–152

Neto I E L, Zhu D Z, Rajaratnam N. 2008. Bubbly jets in stagnant water. International Journal of Multiphase Flow, 34(12): 1130–1141, doi: 10.1016/j.ijmultiphaseflow.2008.06.005

Nissanka I D, Yapa P D. 2016. Calculation of oil droplet size distribution in an underwater oil well blowout. Journal of Hydraulic Research, 54(3): 307–320, doi: 10.1080/00221686.2016.1144656

Niu H, Li Z, Lee K, et al. 2011. Sensitivity of a deepwater blowout model on oil droplet size distribution. In: Proceedings of the 34th AMOP Technical Seminar Environmental Contamination

and Response. Banff (Alta), Canada: Arctic &Marine Oilspill Program, 189–200

Peng Z B, Yuan Z L, Wu X, et al. 2009. Experimental study on drop formation in liquid–liquid fluidized bed. Chemical Engineering Science, 64(6): 1249-1259

Ryerson T B, Camilli R, Kessler J D, et al. 2012. Chemical data quantify *Deepwater Horizon* hydrocarbon flow rate and environmental distribution. Proceedings of the National Academy of Sciences of the United States of America, 109(50): 20246–20253, doi: 10.1073/pnas.1110564109

Tang Liujuan, Masutani S M. 2003. Laminar to turbulent flow liquid-liquid jet instability and breakup. In: Proceedings of the 13th International Offshore and Polar Engineering Conference. Honolulu, Hawaii, USA: ISOPE, 317–324

Yapa P D, Wimalaratne M R, Dissanayake A L, et al. 2012. How does oil and gas behave when released in deepwater? Journal of Hydro-Environment Research, 6(4): 275–285, doi: 10.1016/j.jher.2012.05.002

Zhao Lin, Boufadel M C, Socolofsky S A, et al. 2014. Evolution of droplets in subsea oil and gas blowouts: development and validation of the numerical model VDROP-J. Marine Pollution Bulletin, 83(1): 58–69, doi: 10.1016/j.marpolbul.2014.04.020

Zhao Lin, Shaffer F, Robinson B, et al. 2016. Underwater oil jet: hydrodynamics and droplet size distribution. Chemical Engineering Journal, 299: 292–303, doi: 10.1016/j.cej.2016.04.061

Zheng Li, Yapa P D. 2000. Buoyant velocity of spherical and non-spherical bubbles/droplets. Journal of Hydraulic Engineering, 126(11): 852–854, doi: 10.1061/(ASCE)0733-9429(2000)126:11(852)

Zhu Hongjun, You Jiahui, Zhao Honglei. 2017. An experimental investigation of underwater spread of oil spill in a shear flow. Marine Pollution Bulletin, 116(1–2): 156–166